Surface Heat Budget of the Arctic Ocean

BY TANEIL UTTAL, JUDITH A. CURRY, MILES G. MCPHEE, DONALD K. PEROVICH, RICHARD E. MORITZ, JAMES A. MASLANIK, PETER S. GUEST, HARRY L. STERN, JAMES A. MOORE, RENE TURENNE, ANDREAS HEIBERG, MARK. C. SERREZE, DONALD P. WYLIE, OLA G. PERSSON, CLAYTON A. PAULSON, CHRISTOPHER HALLE, JAMES H. MORISON, PATRICIA A. WHEELER, ALEXANDER MAKSHTAS, HAROLD WELCH, MATTHEW D. SHUPE, JANET M. INTRIERI, KNUT STAMNES, RONALD W. LINDSEY, ROBERT PINKEL, W. SCOTT PEGAU, TIMOTHY P. STANTON, AND THOMAS C. GRENFELD

A year/long ice camp centered around a Canadian icebreaker frozen in the arctic ice pack successfully collected a wealth of atmospheric, oceanographic, and cryospheric data.

The Surface Heat Budget of the Arctic Ocean (SHEBA) is a research program designed to document, understand, and predict the physical processes that determine the surface energy budget and the sea–ice mass balance in the Arctic (Moritz et al. 1993; Perovich et al. 1999). The central motivation behind SHEBA lies in the fact that the Arctic has recently undergone significant changes that are hypothesized to be a combination of poorly understood natural modes of variability and anthropogenic greenhouse warming. In addition, general circulation models (GCMs) have large discrepancies in predictions of present and future climate in the Arctic (e.g., Randall et al. 1998), and consequently, large uncertainties about the how the Arctic influences global climate change. These difficulties are due, in large part, to an incomplete understanding of the physics of the vertical and horizontal energy exchanges within the ocean–ice–atmosphere system. The SHEBA program is based on the premise that improved understanding of physical processes is needed, and that such understanding must be based on detailed empirical observations. The stated objectives of SHEBA are the following:

AFFILIATIONS: UTTAL AND INTRIERI—NOAA/Environmental Technology Laboratory, Boulder, Colorado; CURRY AND MASLANIK—University of Colorado, Boulder, Colorado; MCPHEE—McPhee Research Company, Naches, Washington; PEROVICH AND GRENFELD—Cold Regions Research and Engineering Laboratory, U.S. Army, Hanover, New Hampshire; MORITZ, STERN, HEIBERG, MORISON, AND LINDSEY—University of Washington, Seattle, Washington; GUEST AND STANTON—Naval Postgraduate School, Monterey, California; MOORE—University Corporation for Atmospheric Research, Boulder, Colorado; TURENNE—Canadian Coast Guard, Quebec City, Quebec, Canada; SERREZE AND PERSSON—Cooperative Institute for Research in the Environmental Sciences, Boulder, Colorado; WYLIE—University of Wisconsin—Madison, Madison, Wisconsin; PAULSON, WHEELER, AND PEGAU—Oregon State University, Corvallis, Oregon; HALLE AND PINKEL—Scripps Institute of Oceanography, La Jolla, California; MAKSHTAS—University of Alaska, Fairbanks, Alaska; WELCH—Winnepeg, Canada; SHUPE—Science and Technology Corporation, Boulder, Colorado; STAMNES—Stevens Institute of Technology, Maplewood, New Jersey

CORRESPONDING AUTHOR: Taneil Uttal, NOAA/Environmental Technology Laboratory, R/E/ET6, 325 Broadway, Boulder, CO 80305-3328
E-mail: taneil.uttal@noaa.gov

In final form 13 September 2001

- To determine the ocean–ice–atmosphere processes that control the surface albedo and cloud–radiation feedback mechanisms over arctic pack ice, and to use this information to improve models of arctic ocean–atmosphere–ice interactive processes.
- To develop and implement models that improve the simulation of the present-day arctic climate, including its variability, utilizing coupled global climate models.

The conceptual design and planning of the SHEBA Project were carried out at workshops in the early 1990s as part of the NSF Arctic System Science (ARCSS) program, which also provided primary support for the three phases of SHEBA.

Phase I of SHEBA (1995–96) involved analysis of historical Arctic datasets, preliminary modeling studies, and development of instrumentation that would be suitable for providing critical measurements in the demanding arctic environment. Phase II of SHEBA (1997–99) was a yearlong field experiment (2 October 1997–12 October 1998), on a drifting station in the pack ice of the Arctic Ocean. The observational program emphasized a coordinated, interdisciplinary measurement effort that would provide the necessary information needed to examine the physical processes associated with interactions among the radiation balance, mass changes of the sea ice, storage and retrieval of heat in the mixed layer of the ocean, and the influence of clouds on the surface energy balance. Phase III of the SHEBA program (2000–2002) is presently on going; activities include analysis of the comprehensive observational dataset and incorporation into a hierarchy of models.

This paper describes the goals of the SHEBA II science program, field operations, and the resulting measurements. Some examples of datasets are shown for the full annual cycle as well as for one stormy day in December. The issue of scaling up the ice camp measurements to represent conditions over the Arctic Basin is discussed, and the conditions of the SHEBA year are examined with respect to recent arctic climate. Finally, the objectives of SHEBA phase III are described briefly.

SHEBA GOALS. The central theme of SHEBA emerged based on the premise that improved understanding of physical processes involved in the surface energy budget and air–sea–ice interactions is needed to address the issues of climate feedback in the Arctic, and improve our ability to model arctic climate. Hence the overall goal of SHEBA is to acquire the measurements needed to improve the parameterizations of key processes and to integrate new and improved parameterizations into general circulation and climate models.

To achieve these goals, the SHEBA program was designed in particular to develop a predictive understanding of ice–albedo feedback and cloud–radiation feedback mechanisms, as well as the coupling between them. According to Peixoto and Oort (1992), "The feedback mechanisms act as internal controls of the system and result from the coupling or mutual adjustment among two or more subsystems. Part of the output returns to serve as an input, so that the net response of the system is altered; the feedback mechanism may act either to amplify the final output (positive feedback) or dampen it (negative feedback)." For SHEBA, the hypothesized ice–albedo feedback refers to the process of warmer temperatures, and or decreased ice concentration resulting in lower aggregate surface albedo and increased absorption of solar radiation in the ice and upper ocean, further decreasing the albedo. The hypothesized cloud–radiation feedbacks refers to the mechanisms by which clouds modify shortwave and longwave atmospheric fluxes, the subsequent changes on surface temperature, and the reciprocating effect on the evolution of cloud formation and microphysics. The cloud–radiation feedback can be positive (warming) or negative (cooling) depending on a number of factors, including the season, the amount of condensed cloud water, the size and shape of cloud particles, the phase of the particles, and cloud amount/height. The expectation is that incorporation of realistic representations of these processes into large-scale models will lead to a much more complete understanding of the total sensitivity of the arctic air–sea–ice system to variations in atmospheric and oceanic forcing on seasonal, interannual and longer timescales. The overall SHEBA plan is to collect detailed observational datasets of ocean, ice, and atmosphere quantities over an annual cycle and use the field observations to

- support the analysis and interpretation of physical processes that control the surface heat and mass balance and contribute to ice–albedo and cloud–radiation feedback mechanisms,
- construct and test realistic models and parameterizations of these physical processes on the local and aggregate scales, and
- provide initial condition, boundary conditions, forcing functions, and test data to support SHEBA modeling efforts.

SHEBA was a partner in a multiagency arctic research effort. The research goals overlapped with the

National Aeronautics and Space Administration (NASA) First International Satellite Cloud Climatology Project (ISCCP) Regional Experiment (FIRE)–Arctic Clouds Experiment (ACE; Curry et al. 2001), which conducted an extensive aircraft campaign over the SHEBA ice camp from April to July 1998. The goals of the FIRE–ACE program focus on the interactions between arctic clouds and the surface and radiative properties of spring and summer clouds. Similar to SHEBA, one of the end goals of FIRE–ACE is to improve climate model parameterizations of cloud and radiation processes, with additional emphasis on evaluating satellite retrievals of cloud and surface properties in the Arctic. The Department of Energy's Atmospheric Radiation Measurement (ARM) program (Stokes and Schwartz 1994) collects information on atmospheric cloudiness and radiation from continuously operating surface sites around the globe, with one site situated in Barrow, Alaska (Stamnes et al. 1999). The ARM program contributed a significant suite of surface radiometers that were operated at the SHEBA ice camp. The three programs in combination have jointly been dubbed SHEBA–ARM–FIRE (SAFIRE) and are further described by Randall et al. (1998). Other collaborating programs included the Japanese Marine and Science (JAMSTEC) buoy program, the RADARSAT Geophysical Processor System (RGPS), the Alaska SAR Facility (ASF), the Department of Fisheries Canada, the United States Coast Guard, and the Scientific Ice Expeditions (SCICEX) submarine program of the US Navy and NSF. SHEBA was primarily sponsored by the National Science Foundation (NSF) and the Office of Naval Research.

EXPERIMENT DESIGN. The Arctic is one of the most poorly observed areas of the earth. Because of the long polar nights, extreme cold, and lack of permanent surfaces from which to deploy instruments, the logistics involved with scientific measurements historically have been daunting. Satellites have the potential of providing the necessary spatial and temporal coverage, but many of the algorithms and retrieval strategies that are useful at lower latitudes are not successful in the Arctic. At present, development of satellite techniques to observe arctic clouds, ice, surface temperatures, albedos, and ocean properties are severely limited by the lack of in situ datasets for validating and improving satellite retrievals. This is underscored by the fact that large discrepancies exist between surface- and satellite-derived climatologies (Schweiger and Key 1994; Rossow et al. 1993).

The goals of SHEBA required an interdisciplinary effort with ocean, ice, and atmosphere measurements being made simultaneously, which is in contrast to many previous programs that have been either strictly atmospheric or oceanographic in nature. The SHEBA dataset included observations of the mass balance and physical characteristics of the ice cover, surface energy fluxes including upward and downward radiation at several heights above the surface, vertical structure of the atmosphere, cloud microphysical and optical properties, and upper-ocean conditions. Complicating the data acquisition was the large subgrid-scale horizontal variability in the ice, ocean, cloud cover, and near-surface heat and mass fluxes. Thus an important objective of the field program was also to obtain sufficient data on spatial variability so that local measurements could be scaled up to characterize processes and interactions occurring on larger scales. To address the primary SHEBA objectives, measurements were required that documented the large seasonal changes in the ice mass balance and surface energy balance for a representative region of pack ice and at a variety of local sites that typify the major surface types within the region. Simultaneity and continuity of the measurements were required to initialize, force, and test models of the coupled atmosphere–ice–ocean system as well as to examine the physical processes involving the ice–albedo and cloud–radiation feedbacks.

Annual cycle measurements. The annual cycle is particularly pronounced in the Arctic, where the sun is absent during the winter months, continuously present in the summer months, and at low zenith angles for prolonged periods compared to lower-latitude sites. Wintertime is a period of continual sea-ice growth, counterbalanced by summer with continual ice melt and ablation; the in-between months of spring and fall often are characterized by dramatic transitions in cloud properties, surface fluxes, ice albedos, and upper-ocean properties. Therefore, an important emphasis in the SHEBA project was to make measurements over an annual cycle; these measurements are summarized in Table 1.

Measurements through an ocean–ice–atmosphere vertical column. It was conceptualized that comprehensive observations should be made through a column reaching from the top of the troposphere (~12 km above the surface) down to the ocean pycnocline (~0.5 km below the surface). This column serves as an observational proxy for a single GCM grid cell so that parameterizations of key physical processes could be tested in single column models (SCMs). Measurements in the column include such diverse

Table 1. Annual cycle measurements.

Instrument	Collection start date	Collection end date	Data product
Deep ocean SeaCat CTD	12 Oct 1997	21 Sep 1998	Ocean depth, temperature, salinity, conductivity, density
Doppler sonar	26 Nov 1997	2 Oct 1998	Upper-ocean current
YoYo CTD (Seabird 911+)	11 Oct 1997	1 Oct 1998	Ocean temperature, conductivity, salinity, density
Dual-thermistor thermal	7 Oct 1997	22 Sep 1998	Thermal microstructure dissipation rate dissipation package
Turbulence mast	9 Oct 1997	26 Sep 1998	Ocean current speed/direction, temperature, salinity, salinity flux, turbulent heat flux, Reynolds stress
ARGOS drifter buoys (microCAT)	2 Oct 1997	2 Oct 1998	Conductivity, salinity, temperature, position
Buoys (thermistors)	14 Oct 1997	10 Feb 1998	Air and snow temperature, position
Buoys (thermistors)	26 Oct 1997	1 Oct 1998	Ice thickness
Snow gauges	11 Oct 1997	1 Oct 1998	Snow depth
Thermistors	13 Oct 1997	1 Oct 1998	Snow and ice temperature
Stress meters			Ice stress
GPS	1 Oct 1997	11 Oct 1998	Ice camp position and heading
Surface weather reports	29 Oct 1997	9 Oct 1998	Cloud-base height, visibility, cloud fraction, wind speed and direction, air temperature, dewpoint, pressure, pressure tendency, weather conditions
Nipher-shielded snow gauge	29 Oct 1997	9 Oct 1998	Liquid water equivalent precipitation
Optical rain gauge	1 Oct 1997		Precipitation rate
Portable Mesonet (PAM) stations	1 Nov 1997	1 Oct 1998	Pressure, temperature, relative humidity, wind speed and direction, broadband shortwave and longwave fluxes up and down
Scintillometer	20 Oct 1997	2 Aug 1998	Refractive index structure, inner scale of turbulence
10-m towers (thermometers, prop anemometers)	9 Oct 1997	1 Oct 1998	Temperature, dewpoint, wind speed and direction at 2 and 10 m, pressure
20-m tower (thermometers, anemometer)	1 Oct 1997	1 Oct 1998	Temperature, relative humidity, wind speed sonic and direction, friction velocity, sensible heat flux, surface and snow/ice temperature
Eppley radiometers	1 Oct 1997	1 Oct 1998	Broadband shortwave and longwave fluxes, down and up
35-GHz cloud radar	20 Oct 1997	1 Oct 1998	Radar reflectivities, Doppler velocities and spectral widths
523-nm depolarization lidar	1 Nov 1997	8 Aug 1998	Lidar backscatter, depolarization ratios
GLAS (Vaisala) rawinsonde	16 Oct 1997	15 Oct 1998	Pressure, temperature, relative humidity, wind speed and direction, position

quantities as ocean temperature, currents, salinity, diffusivity, and heat fluxes; snow depth and stratigraphy; ice temperature, thickness, and albedos; atmospheric precipitation, temperature, radiative fluxes, winds, humidity, and clouds. These simultaneous observations of the mass balance and physical characteristics of the ice cover, and atmospheric and oceanic heat fluxes, are key processes that determine the energy exchanges in the arctic ocean–ice–atmosphere system. In Tables 1–3 the entries are arranged approximately in order from the base of the SHEBA column to the top.

Measurements over local to Arctic Basin scales. Previous observations in the Arctic Ocean surface indicated that surface temperatures, albedos, energy fluxes, and ice thickness exhibit large variations on horizontal scales of tens to hundreds of meters, far smaller than grid cells of even the highest-resolution GCM. A major challenge in the design of the SHEBA field experiment was to bridge the scale gap between local scales measured at the ice station and the "aggregate" scale at which the results become relevant to a single column in a climate model. Thus, to achieve SHEBA goals, a coordinated observation effort was necessary on three different spatial scales:

- *Local scale (<10 km).* Measurements made on this scale were conducted in the vicinity of the ice station with the purpose of documenting detailed local physical processes in the ocean, ice, and atmosphere for a variety of ice conditions experiencing seasonal ocean and atmosphere changes throughout the year.
- *Aggregate scale (10–100 km).* This scale characterized ice thickness distributions, mesoscale cloud systems, and high-resolution general circulation model grid cells. Sampling at this scale documented the spatial variability in the ice, ocean, and atmosphere.
- *Basin scale (1000 km+).* This scale required that local and aggregate measurements be examined in context of applicability to the entire Arctic Basin.

Logistics dictated that the bulk of the measurements be made on the local scale, usually within 5 km of the ship. A buoy array, research aircraft, helicopter surveys, and submarine transects were made on the aggregate scale, and satellite observations extended observations over the entire Arctic Basin. Seasonal measurements that were only feasible or necessary for shorter time periods are summarized in Table 2. Measurements from collaborating programs are shown in Table 3.

Modeling. SHEBA Phase I and Phase II supported preliminary work with process models on a number of topics including ice thickness distributions, formation and evolution of meltponds, parameterizations of turbulent surface fluxes over sea ice, upper-ocean and sea-ice energy exchanges, and lead effects on atmospheric budgets of sensible heat, water vapor, and condensate. The majority of the modeling work is being performed as a part of SHEBA Phase III and is incorporating a hierarchy of process models, regional models, large eddy simulation models (LES), SCMs and GCMs for the ocean, the ice, and the atmosphere, both in standalone and coupled incarnations. The Phase III modeling studies, as well as a number of data processing projects, are briefly discussed at the end of this paper.

Ancillary experiments. Because of the opportunity that SHEBA provided for arctic research, it was also utilized as a platform of opportunity for research that was not directly related to SHEBA goals. The largest program, which was arranged in cooperation between NSF and the Canadian Department of Fisheries and Oceans, was a comprehensive ancillary biology program. The overall objective of this program was to measure the carbon flow through the Arctic Ocean, from the exchange of oxygen and carbon dioxide with the atmosphere to the sinking of organic matter out of the upper ocean. Because contaminants enter the Arctic via long-range atmospheric transport and are concentrated up the food chain by the carbon flow, extensive sampling for mercury and persistent organic pollutants was made in the air, water, and biota.

The complex experimental design of SHEBA was formulated to promote synthesis and integration of the observations with models over a range of time- and space scales. The ice station observations were designed specifically to generate comprehensive observational datasets that could be used to test detailed process models that would lead to parameterizations that could be tested in SCMs. The expectation is that incorporation of these improved parameterizations into large-scale models will lead to a much more complete understanding of the total sensitivity of the arctic air–sea–ice system to variations in atmospheric and oceanic forcing on seasonal, interannual, and longer timescales, and that these models will then be useful in assessing the impact of the arctic climate on global climate.

FIELD OPERATIONS. Historically, the Arctic is a region where exploration and scientific objectives have been inextricably linked; landmasses such as Franz Josef Land were still being discovered (often inadvertently by lost explorers) in the late 1800s, and

Table 2. Seasonal measurements.

Instrument	Collection start date	Collection end date	Data product
Seabird SBE-25 CTD	10 Jun 1998	4 Aug 1998	Temperature, pressure, salinity, conductivity down to 60 m in leads
Seabird SBE-19 CTD	6 Jun 1998	9 Aug 1998	Temperature, pressure, salinity, conductivity at lead surface and down to 15 m in leads
AC-9	17 Jun 1998	4 Aug 1998	Optical properties, beam attenuation, absorption coefficient in leads
Eppley radiometer	7 Jun 1998	1 Aug 1998	Lead albedo
Buckets/filters	8 Oct 1997	4 Oct 1998	Beryllium-7 concentration
Mobile radiometric platform (IR thermometer, thermistor, pyranometers)	5 Apr 1998	8 May 1998	Air and snow temperature, albedo, flux—over ice, snow, and lead surfaces
Electromagnetic induction EM-31	2 Oct 1997	10 Oct 1998	Ice thickness distribution estimates
0.4-μm nucleopore filters	9 Apr 1998	14 Jul 1998	Soot content in snow and ice
Spectron engineering SF-590	11 Jun 1998	3 Sep 1998	Spectral albedo (300–2500 nm)
Zipp and zonen radiometer	1 Apr 1998	27 Sep 1998	Wavelength-integrated albedo
Magneprobe radar	25 Mar 1998	11 May 1998	Spatial (not temporal) snow cover
Geokon vibrating wire stress meters	1 Jun 1998	31 Aug1998	Ice stresses
Helicopter aerial photography	17 May 1998	4 Oct 1998	Photos of surface in 250 frames/flight: 5/17, 5/20, 6/10, 6/15, 6/22, 6/30, 7/08, 7/15, 7/20, 7/25, 8/7, 8/22, 9/11, 10/4
Helicopter IR photometry	10 Jun 1998	29 Aug 1998	IR photometry
Twin otter surface property survey	14 Oct 1997	11 May 1998	Surface temperatures and video
Tethered balloon (Vaisala T/RH/ wind sensors)	4 Dec 1997	19 July 1998	Pressure, temperature, relative humidity, wind speed and direction
Tethered balloon (cloud particle videometer)	5 May 1998	12 Oct 1998	Cloud particle sizes and concentrations
Tethered balloon (radiometer)	14 Sep 1998	21 Sep 1998	Hemispheric radiation

the Northwest Passage was not navigated until 1905. The beginning of scientific field experiments in the modern sense, with a primary emphasis on measuring physical properties of the arctic environment, can probably be assigned to the year 1937 when the Russians established a drifting ice camp composed of fur-lined tents. This camp, designated North Pole 1, was the first in a series of 31 long-term, research ice camps, which where consecutively designated NP1 to NP31. The NP camps were typically deployed by icebreaker

Table 3. Measurements made by collaborating programs

Instrument	Collection start date	Collection end date	Data product
SCICEX submarine	28 Sep 1997	1 Oct 1997	Ice thickness distribution, sonar ice drift profiles
Buoys	1 Oct 1997	1 Oct 1998	CTD data, mooring data
IOEB buoys (thermistors, R. M. Young probes, etc.)	30 Sep 1997	1 Oct 1998	Pressure, temperature, winds speed and direction, ice temperature profiles, biogeochemical data, position
IOEB buoys (CTD, ADCP)	30 Sep 1997	1 Oct 1998	Ocean temperature, salinity, ocean current profiles
Radiometers	1 Nov 1997	30 Sep 1998	Upwelling radiation and downwelling radiation
SkyRad (radiometers)	1 Nov 1997	30 Sep 1998	Downwelling radiation
Atmospheric emitted radiance interferometer (AERI)	25 Oct 1997	1 Jul 1998	Downwelling spectral radiances
Multifilter rotating shadowband radiometer	25 Oct 1997	30 Sep 1998	Downweling irradiances
Whole sky imager	25 Oct 1997		Visual images of atmospheric conditions
Microwave radiometer	25 Oct 1997	9 Sep 1998	Brightness temperatures at 23.8 and 31.4 GHz, integrated liquid water path, integrated water vapor path
Laser ceilometer	25 Oct 1997	30 Sep 1998	Cloud-base heights
Standard filter ozonemeter			Ozone concentrations
NASA Polar Pathfinder APP products (AVHRR)	1 Nov 1997	31 Oct 1998	Brightness temperature, surface temperature, radiance, albedo, solar zenith angle, surface type
Satellite (NOAA polar orbiter–AVHRR)	16 Sep 1997	1 Oct 1998	IR composite image
Satellite (SAR)	1 Nov 1997	8 Oct 1998	Ice motion and deformation
Satellite (SAR)	1 May 1998	15 Oct 1998	Floe size distribution
Satellite (RADARSAT)	1 Nov 1997	31 Oct 1998	Ice motion products
Satellite (RADARSAT)	1 Nov 1997	8 Oct 1998	Images and derived products

and supported by aircraft, and the standard tour of duty for the hardy inhabitants of these ice camps was 1 yr; the efforts of these Russian scientists resulted in a 54-yr-long record of measurements (Kahl et al. 1999). The U.S. drifting ice camp program started with the manning of ice island T3 in early 1950. Since then there have been over 50 ice camps deployed in various regions of the Arctic; most have been short-term, air-deployed, springtime operations when the combination of sunlight and sea-ice conditions optimized the environment for temporary human habitation.

Ships frozen into the ice have also been deployed for research with mixed results. In 1892 the *Fram,* under the leadership of Fridtjof Nansen, made a successful 3-yr drift across the polar basin collecting a wealth of scientific data. In the first part of this cen-

tury, Roald Amundsen's drift in the *Maud* along the east Siberian Sea was a successful scientific endeavor as well, although disappointing to him, as his goal had been to drift to the North Pole and beyond. In 1937 the Russian supply ship, the *Sedov,* was inadvertently trapped in the ice and started to drift north. A decision was made to convert her into a drifting research site platform, which drifted free two years later in the Fram Strait.

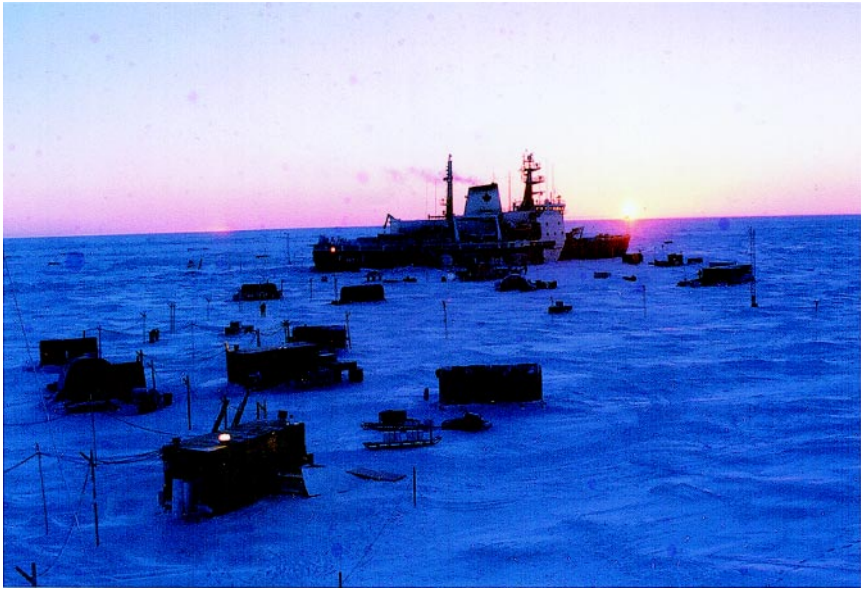

Fig. 1. The SHEBA ice camp in Oct 1997 immediately after setup. (Photo credit: Don Perovich.)

During SHEBA, the Canadian Coast Guard Ship *Des Groseilliers* was frozen into the ice at 75°N, 142°W about 570 km north and east of Prudhoe Bay, Alaska. The choice of a ship-based experiment was mandated not only by the number of people and experiments that were projected for SHEBA but the power requirements that otherwise would have had to be provided by diesel generators on the ice. The ship served as command center, power station, hotel, laboratory, staging area, and machine shop for the various SHEBA projects both on the ship's decks and on the ice surrounding the ship. The ship option was also determined to be the safest considering the number of personnel that would be rotating in and out of the ice camp. The camp was installed in the fall of 1997 with the aid of a second Canadian icebreaker, the *Louis St. Laurent,* as the amount of equipment, supplies, and fuel greatly exceeded the cargo capacity of the *Des Grosseilliers* alone.

Since ships are not routinely frozen into the arctic ice pack, there were many logistical issues surrounding unforeseen conditions that might occur during the intense cold of a prolonged arctic night. As a precaution, oil-fired space heaters were carried to supplement the hot water and electric heating, portable pumps were carried to allow the crew to draw seawater from holes drilled into the ice in the event that intakes were blocked by accumulated ice, and a survival container was carried with sufficient resources to provide shelter against the elements for up to 100 persons living on the ice. The *Des Groseilliers* was packed with enough dry and frozen food to survive 16 months without need for resupply and from the time it left its home port of Québec City in July 1997 until it returned there in November 1998, the only provisions to be airlifted to the ship were fresh fruit and vegetables and other nonessential perishables.

Transportation to and from the ship was accomplished through the use of Twin Otter aircraft that have the ability to take off and land on wheels, skids, or floats with extremely short runways. During the first 9 months of the drift, when aircraft support was used, seven runways of about 1000 ft × 60 ft were built or rebuilt supporting 57 landings and takeoffs. Most crew changes occurred after 6 weeks, with occasional 3-week rotations during special periods of setup and intensive observations. After the ice station drifted too far north, and the ice conditions became too treacherous for aircraft landings, the United States Coast Guard sister ships *Polar Star* and *Polar Sea* were utilized to complete personnel transfers. Radio communications with the land became unreliable as the ship drifted far to the west and north, but communications were maintained throughout the project utilizing INMARSAT-B satellite links.

The ice camp (Fig. 1) around the ship was comprised of numerous tents, seatainers, plywood structures, and towers that housed the bulk of the oceanographic, meteorological, and logistics operations. In addition, there were 960 50-gallon drums of various fuels for the ship, helicopters, and snow machines. This situation was of course vulnerable to lead activity and the unpredictable pattern of summertime melting. Significant resources

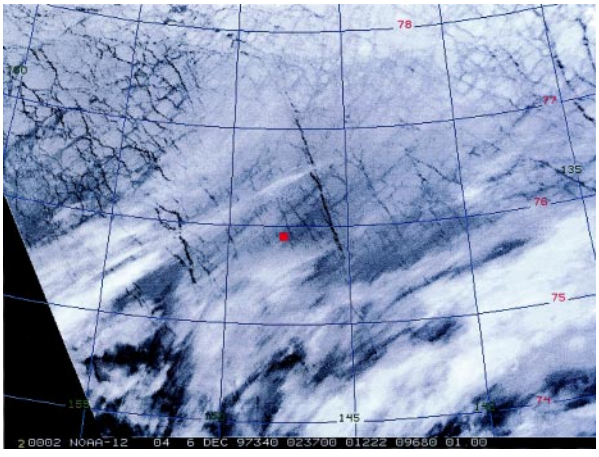

FIG. 2. Satellite image (0237 UTC 6 Dec) indicating elongated clouds over the ice camp (red square) that thicken to the south and clear to the north. The patterns in the ice are presumed to be old lead fractures that have frozen. The SHEBA ice camp is at 75°53′N and 148°15′W.

were continually being applied to the problem of constant relocation of equipment and buildings as they came in danger of sinking or falling through the ice. It was fortunate that the 20-m meteorological tower, which was the only installation that could not have been relocated, was the only one that managed to stay in its original location for the entire drift.

Throughout the year, the ship drifted over 1200 n mi through the Arctic Ocean. Two hundred scientists, a handful of media personnel, and 70 members of the Canadian Coast Guard lived at the station, with tours of duty ranging from two days to one individual who was on site for the entire experiment. Thirty-thousand meals were prepared, 3000 tons of freshwater were produced by desalinating ocean water, and the SHEBA experiment resulted in 374 scientifically productive days adrift in the Arctic Ocean without serious losses or damage to equipment or personnel.

PRELIMINARY OBSERVATIONS. This section is divided into three parts, highlighting example measurements from the SHEBA project. The first part concentrates on 7 December 1997, which was a particularly interesting storm event, and demonstrates some of the detailed measurements made through the SHEBA column. The second shows examples of measurements for the full annual cycle and previews some of the difficulties that will be encountered in untangling seasonal changes from the changes that resulted from the nonstationary ice station drifting through different oceanic and atmospheric regimes. The final part showcases examples of some of the seasonal and ancillary measurements for which the *Des Grosseilliers* provided a platform of opportunity. The purpose of this section is primarily to provide examples of the kinds of data that are available from the SHEBA project; the quantitative, scientific analyses of these datasets are the subject of a number of ongoing papers, many of which will be part of a SHEBA special issue of the *Journal of Geophysical Research,* a FIRE–ACE special issue of the *Journal of Geophysical Research,* as well as the future research that will be a part of SHEBA III.

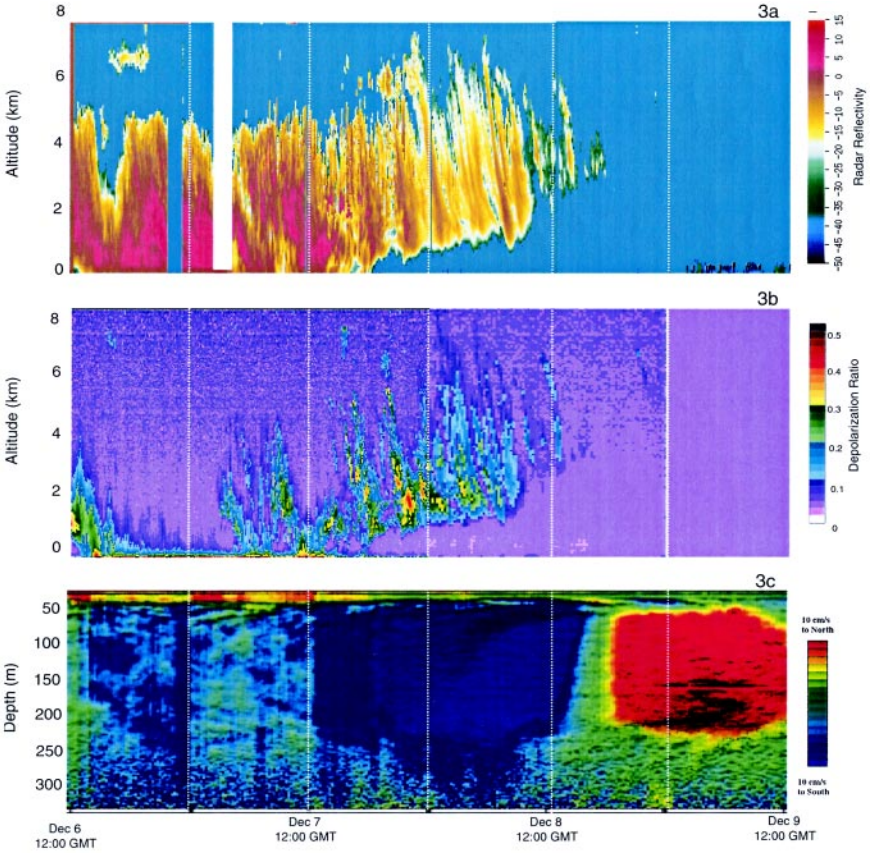

FIG. 3. Time–altitude/depth cross section of (a) radar reflectivity, (b) lidar depolarization, and (c) Doppler sonar ocean currents from 1200 UTC 6 Dec to 1200 UTC 9 Dec.

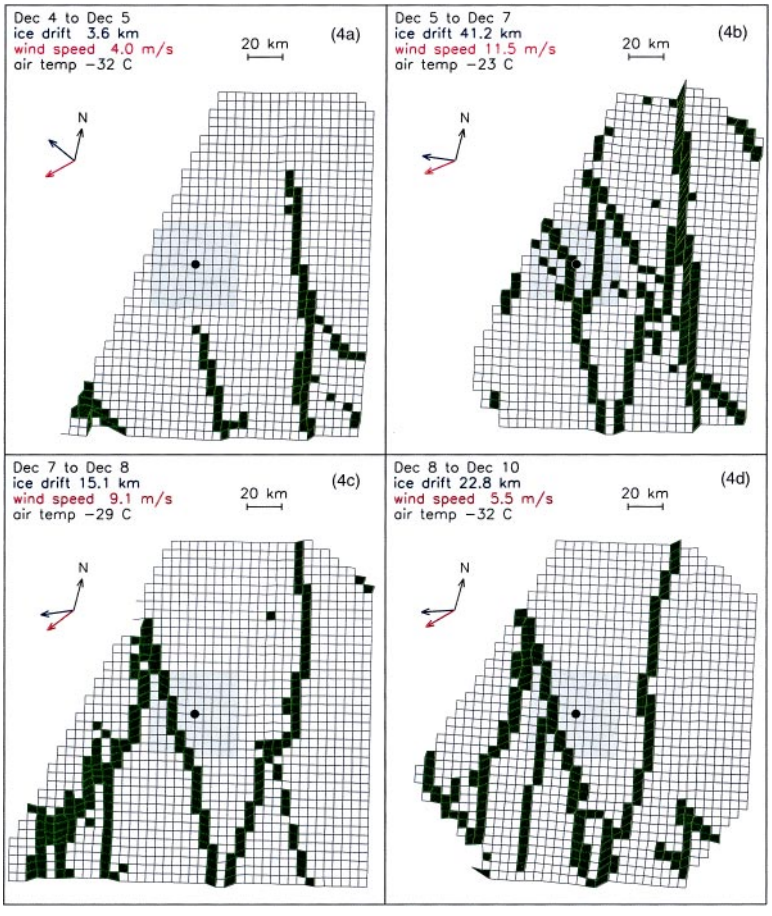

FIG. 4. Sea-ice deformation near the SHEBA ice camp from 4 to 10 Dec 1997. The ship is located at the black dot in the center of each panel. Green (deforming) cells show the pattern of active leads. These are derived from successive Radarsat SAR images from RGPS.

Measurements through the SHEBA column around 7 December 1997. By 7 December, the transition to winter conditions was well under way. The sun had set for the polar night on 6 November, the snow cover was growing deeper with depths ranging from 0.02 to 1.0 m, and the sea ice had cooled in response to the cold winter surface air temperatures that were ranging from average daily maximums of –25°C to minimums approaching –40°C. The net surface radiative fluxes had been negative (cooling) since the meteorological tower had been erected in late October. A storm buffeted the ice camp from 5 to 9 December, and the ocean was turbulent, with 7 December being the most energetic day. The SHEBA ice station was on the edge of a very large high pressure system to the northwest that dominated the northern Chukchi Sea up to the pole and a small low had formed to the southeast along the Alaskan coast. The ice station experienced strong northeasterly winds of 20–25 kt that caused obscured visibility from blowing snow. A satellite image (Fig. 2) showed that the ice station was on the northern edge of a cloudy boundary on 6 December, with clear skies to the north and thicker cloud cover to the southeast. The clouds were moving from the southwest and evaporating over the ship, and the cloud boundary did not advance northward, rather it regressed slightly southward as a trough formed in the upper air north of the ice station on 8 December.

By 1330 UTC on 6 December, the 35-GHz cloud radar indicated cloud solid echo from the surface to about 5 km above ground level (AGL), which persisted until about 1830 UTC on 7 December (Fig. 3a). At 1830 UTC, both the cloud radar and the depolarization 532-μm lidar (Fig. 3b) indicated a rising cloud base and dissipating clouds with completely clear skies by 1800 UTC on 8 December. These cloud measurements at the ice camp are compatible with the regressing cloud boundary indicated by the satellite measurements. Lidar transmitted/received depolarization ratios provide an assessment of the cloud phase, with spherically symmetric particles (water droplets) backscattering incident energy through a combination of axial reflections and surface waves that do not change the incident polarization state, thus resulting in low depolarization ratios (<0.1). More complex shapes usually associated with ice crystals induce internal reflections that rotate the incident polarization state resulting in higher depolarization ratios (>0.1). The lidar depolarization ratios on 6 December ranged from 0.03 to 0.43 indicating that the cloud was both liquid and ice phase, with depolarization ratios less then 0.1 predominating; this combined with the clear attenuation of the lidar signal at levels well below highest radar echoes indicating that for most of the period variable amounts of liquid water were present at different levels in the cloud.

The upper ocean was particularly energetic as indicated by the meridional oceanic velocity relative to the earth measured by the 140-kHz Doppler sonar (Fig. 3c). Prior to 6 December, downward-propagating internal waves were detected, and the large-scale background meridional velocity was small. At 1400 UTC on 7 December the meridional flow became stronger and southerly, and then shifted rapidly to a

strong northward velocity at 1200 UTC on 8 December. This indicates that the ice station passed over a cyclonic vortex. Such vortices typically extend between the base of the mixed layer (or higher), and approximately 200–300-m depth (Manley and Hunkins 1985).

Figure 4 shows the deformation of the sea ice in the vicinity of the ice station from 4 to 10 December, computed from NASA's Radarsat Geophysical Processor System (RGPS) that maps the sea-ice motion on a regular 5-km grid from sequential RadarSAT Synthetic Aperture Radar (SAR) images, and uses the relative motion of the grid to produce the pattern of active leads (Stern and Moritz 2001). Green indicates grid cells deformed by more than 15%, with the ship marked by a black dot in the center of each panel. The relative ice drift and wind speed vectors are indicated in the upper-right-hand corner of each panel. From 4 to 7 December the wind speed increased from about 4 to 11.5 m s^{-1}, then gradually decayed to 5.5 m s^{-1} by 10 December, blowing consistently from NE to SW (red arrows). The ice drifted generally westward (blue arrows). Figures 4a and 4b show leads propagating from the south to north and forming characteristic diamond patterns with angles of intersection of 35°–45°. The sea-ice deformation events of 5–7 and 7–8 December resulted from shearing motions (4% and 6% day^{-1}, respectively) with only a small amount of convergence (less than 0.2% day^{-1}). From 8 to 10 December the sea ice in the SHEBA column diverged by 1.3% day^{-1}, adding 33 km^2 of new lead area in the vicinity of the ship.

Figure 5 shows the temperature and velocity profiles through the depth of the SHEBA column as measured by a number of atmospheric, ice, and oceanographic sensors that are arranged vertically from the top of the atmosphere down to 600 m below the ocean surface. The temperature profiles (in red, with the addition of other colors for multiple temperature profiles for different kinds of ice) have been arranged so that the end points approximately match at the ocean–ice, ice–atmospheric boundary layer, and atmospheric boundary layer–troposphere interfaces. Temperatures in the troposphere and lower stratosphere (Fig. 5a) are mea-

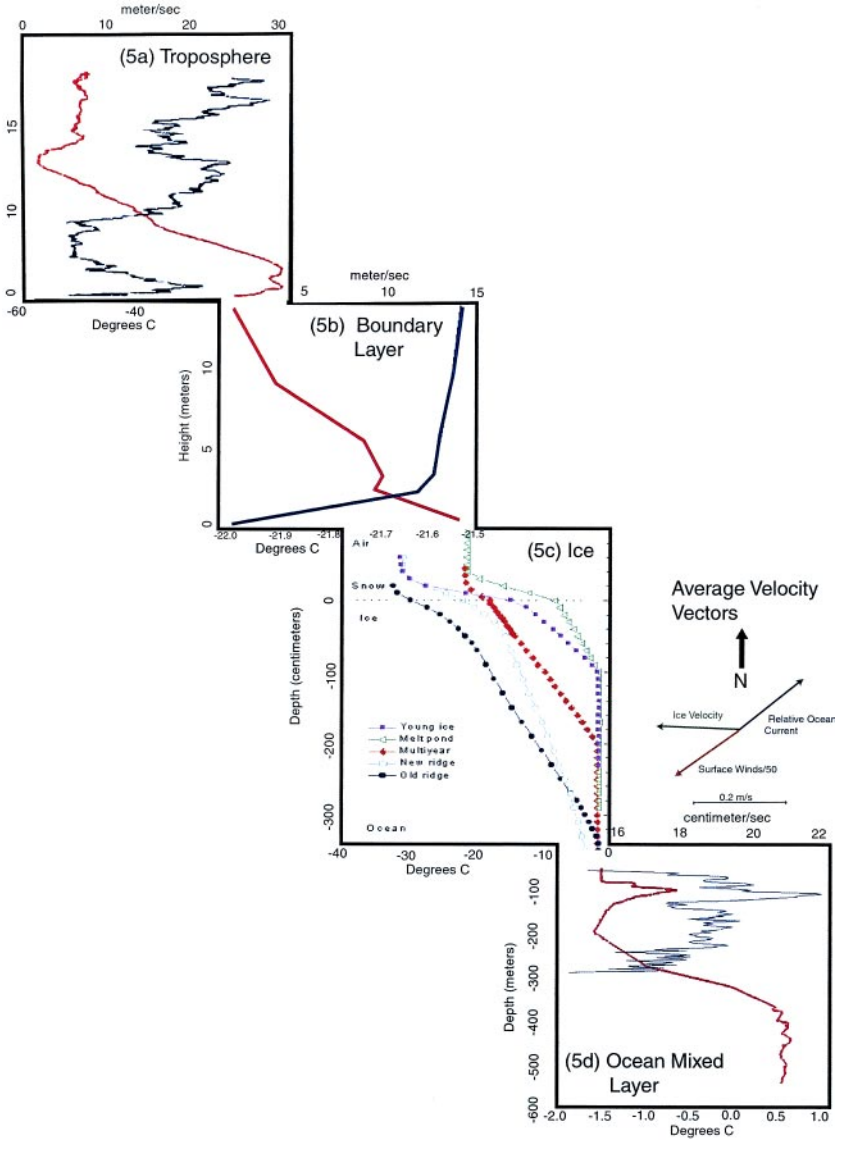

FIG. 5. Temperature and velocity profiles through the SHEBA column on 7 Dec 1997. (a) Rawinsonde temperature (red) and wind speed (blue), (b) 20-m meteorological tower temperature (red) and wind speed (blue), (c) ice thermistor temperature at a variety of sites, and (d) ocean CTD temperature (red) and Doppler velocity current speed (blue). Relative velocity vectors for surface wind, ice drift, and ocean current are shown to the right of (c).

sured by rawinsonde, in the atmospheric boundary layer (Fig. 5b) by thermometers on the 20-m meteorological tower, in the ice (Fig. 5c) with ice thermistors, and through the upper ocean (Fig. 5d) with temperatures measurements made by a winched conductivity–temperature–diffusivity (CTD) system. An important purpose of this figure is to demonstrate the range of scales that must be integrated in the analysis of ocean–ice–atmosphere column both in temperature range and vertical scales. The temperature scales (on the lower axis of each panel) range from tenths of a degree in the atmospheric boundary layer, to 1–2 degrees in the ocean mixed layer, to tens of degrees in the ice and the troposphere, with a total temperature range throughout the column of +0.5°C at 550 m below the ocean surface to –57°C at about 13 km AGL. The vertical scales are equally variable; 300 cm in the ice panel, 20 m in the atmospheric boundary layer, 600 m in the ocean, and finally, 20 km for the troposphere/lower stratosphere panel.

Within the sea ice, there were significant variations in the temperature profiles (Fig. 5c) as a function of ice type; the different profiles are shown for five sites: young ice, ponded ice, undeformed multiyear ice, a new ridge, and an old consolidated ridge. The "cold front" had already reached the bottom of all of the sites except for the 6–8-m-thick new ridge, with temperature profiles ranging from about –30°C at the surface to –2°C at the bottom of the ice. The winter growth season was well under way with ice growth rates from 0.5 to 1.0 cm day^{-1}, with the exception of the underside of the thick ridge that was ablating rather than growing. Interestingly, the rate of growth of the young ice was so great that its thickness was equal to that of the ponded ice by 7 December.

Figure 5 also shows profiles of wind speeds (panels a and b) and relative ocean currents (panel d), which are plotted in blue with scales at the top of each panel. Wind speeds in the troposphere (from rawinsonde) indicated a low-level jet of 20 m s^{-1} at 1 km AGL; high near-surface winds were also detected by anemometers on the meteorological tower, showing winds of 13 m s^{-1} just 3 m above the surface, resulting in a well-mixed surface layer with a log-z wind speed profile. The Doppler sonar showed a turbulent ocean with strongly sheared velocities ranging from –15 to –22 cm s^{-1}. Next to the ice panel (Fig. 5c), the relative velocity vectors between the surface winds, the ice speed, and the ocean currents are shown; note that the atmospheric wind vector is scaled by a factor of 50 to fit on the same diagram as the ice and ocean velocity vectors. During the 3-day period between 6 and 9 December, the ice station moved about 60 km in a generally westward direction.

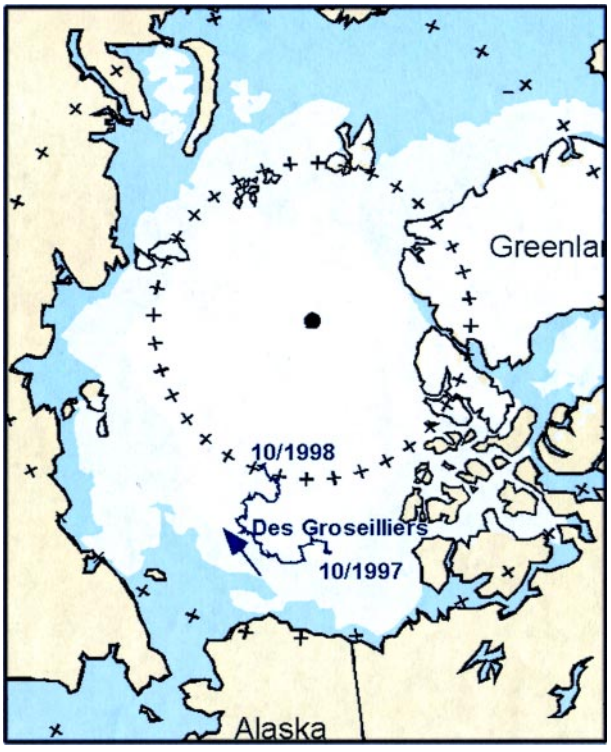

FIG. 6. The yearlong SHEBA drift. Blue zigzag line extending from Oct 1997 to Oct 1998.

Measurements of annual cycles. During the course of the SHEBA experiment, the ice camp drifted from an original location north and east of Prudhoe Bay, Alaska, on October 1997 in a mostly westerly direction from October to May, at which time it began moving mostly north until the end of the project in October 1998 (Fig. 6). This drift pattern was not completely unexpected based on the location of the camp within the Beaufort Gyre, although the camp ended in a location farther north and east than had been predicted based on historical buoy data.

Figure 7 shows examples of some of the time series measurements that were made for the entire annual cycle, again arranged approximately from the top of the atmosphere down to the ocean. Beginning at the top, Fig. 7a shows examples of satellite-derived cloud-top temperatures and layer-average cloud particle effective radii that were generated by applying the Cloud and Surface Parameter Retrieval system to Advanced Very High Resolution Radiometer (AVHRR) Polar Pathfinder gridded and calibrated radiances (Han et al. 1999; Maslanik et al. 2001). The individual 5-km values are averaged over a 50 km × 50 km region centered on the SHEBA field site. This and the SAR data shown in Fig. 4 are an extremely small

sample of the satellite products that were available during SHEBA. Additional sensors including the Television Infrared Observational Satellite (TIROS) Operational Vertical Sounder (TOVS), the Special Sensor Microwave/Imager (SSM/I), and visible band imagery from the U.S. National Imagery and Mapping Agency. From these systems a wide range of products is available describing surface and atmospheric conditions. These satellite measurements will be invaluable in generalizing the SHEBA measurements to aggregate and basin scales in future analyses.

In Fig. 7b, the percent of time during which there was cloud over the ice station, and the percent of those clouds that contained some liquid water is shown. The fractional cloudiness was calculated by finding the percent of time that either the 35-GHz cloud radar or the 523-μm cloud lidar had returned signal at any level over 10-day periods. These statistics therefore include a wide range of possible cloud types including tenuous ice fogs at the surface, surface boundary layer clouds, midlevel stratus, cirrus, and precipitation. In general, the ice station was persistently cloudy, especially in the spring and summer when clouds were observed between 80% and 100% of the time. These numbers of fractional cloudiness are somewhat higher than would be extrapolated from historical observations of arctic cloudiness (Vowinkel and Orvig 1970; Warren et al. 1988); however, there are a number of reasons that could account for this including surface observer underestimates due to poor illumination, noninclusion of ice fogs, and poor detection of clouds by satellites, especially during the polar night. Preliminary analyses indicate that the predominant and most radiatively significant clouds were the low-level boundary layer clouds that contained often supercooled liquid water. Somewhat more unexpected than the persistence of cloudiness was the fact that the depolarization measurements from the 523-μm lidar indicated that liquid water was present frequently in these clouds, even during the coldest months of winter when atmospheric boundary layer temperatures were tens of degrees below freezing (Intrieri et al. 2001). Detailed microphysical characteristics of the ice and liquid clouds that occurred during the April–May FIRE–ACE aircraft campaigns are described by Shupe et al. (2001).

The existence of the ubiquitous inversion layers over different regions of the Arctic has been characterized by a number of researchers (e.g., Kahl 1990; Serreze et al. 1992), and it is thought that the predomi-

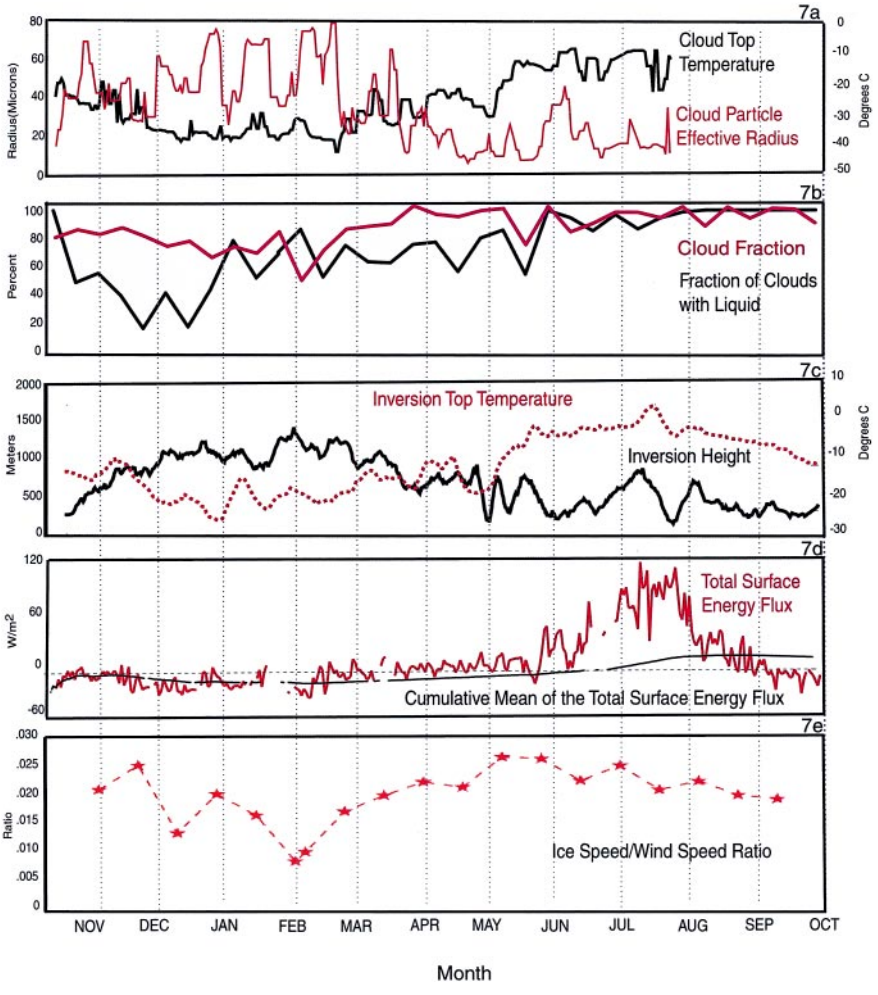

Fig. 7. Yearlong time series (a) cloud-top temperature and mean cloud particle radius from AVHRR Polar Pathfinder, (b) cloud fraction (percent) from 35-GHz cloud radar/depolarization lidar and percent of clouds with liquid water layers, (c) inversion top temperature and inversion top height from rawinsonde, (d) total net surface energy flux and cumulative mean of the total net surface energy flux from the 20-m tower, and (e) ratio of ice speed to wind speed.

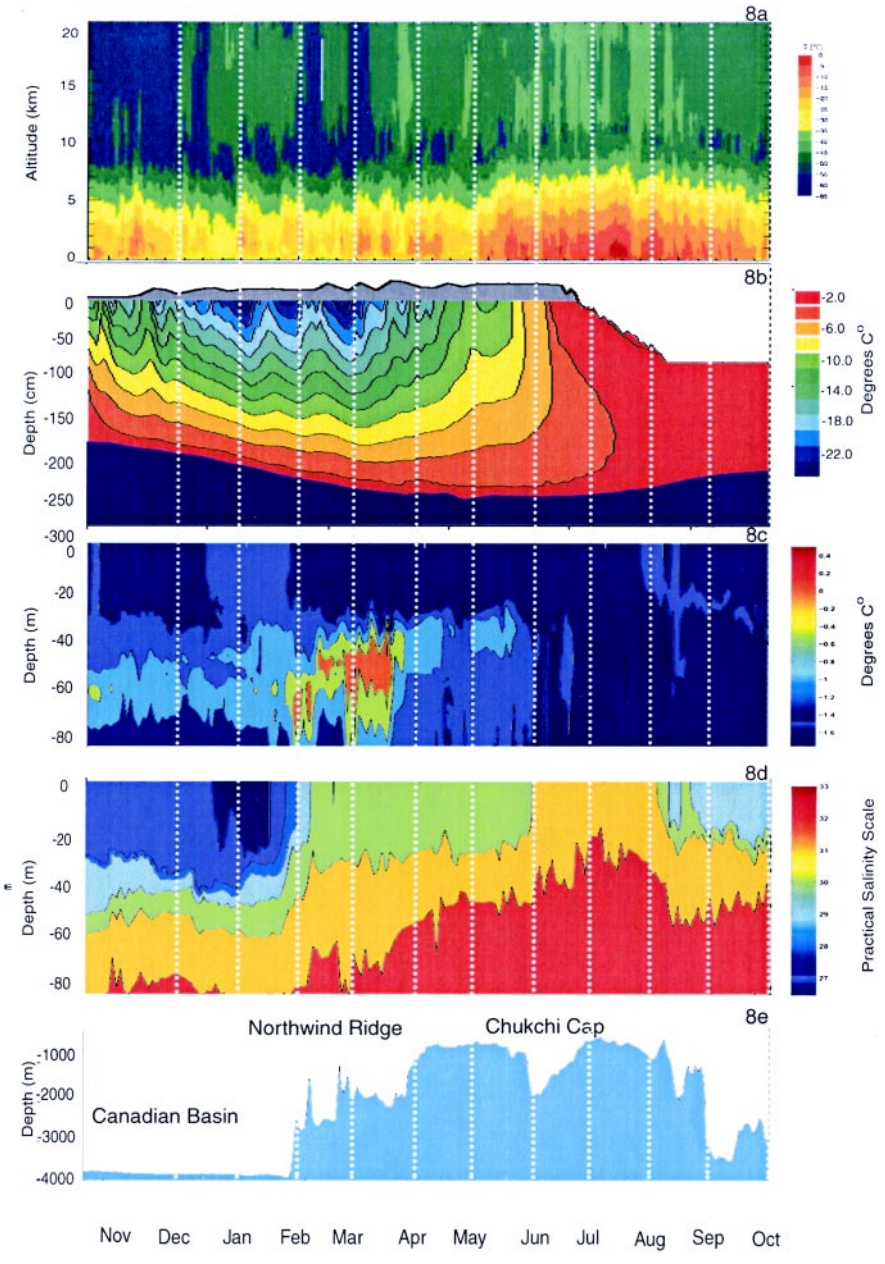

Fig. 8. Yearlong series of vertically resolved measurements: (a) rawinsonde temperatures, (b) ice temperatures and thickness with snow depth in gray (same cm scale), (c) ocean CTD temperature, (d) ocean CTD salinity, and (e) bathymetry.

nant physical mechanisms that contribute to inversion formation in the Arctic include radiative cooling, warm air advection, subsidence, as well as the melting of the ice surface, and cloud processes and turbulent mixing (Curry 1983). Figure 7c shows preliminary calculations of inversion heights and inversion top temperatures for SHEBA from the corrected rawinsonde data. In this analysis, the inversions were often complex and multilayered, and in general, the primary temperature maxima in the lowest 2 km of the atmosphere was used to define the top of the inversion. Inversions were deepest (~1.2 km AGL) and had the coldest tops (~–25°C) during the winter season, but were still persistent, although shallower (~400 m AGL) and warmer (~–5°C) in the summer. The total temperature change through the depth of the inversion was also greater in winter, about 10°C, as opposed to summer, when the temperature change across the inversion was about 5°C. The strong shallow inversions over the ice pack helped keep the air near the surface saturated with respect to ice most of the time (Andreas et al. 2001).

Figure 7d shows the total net surface energy flux and the cumulative running mean of the total net surface energy flux calculated from the beginning of the year. These values, as well as all of the individual turbulent flux, shortwave, and downward components, were calculated using the radiometric, temperature, and sonic anemometer data from the 20-m tower. The net energy flux varied from –35 W m^{-2} in winter to +110 W m^{-2} in the summer, with large day-to-day variations. The running mean of the net flux shows that over the annual cycle, an energy deficit existed until mid-June, at which time an annual energy excess began that persisted to the end of the project. This excess net energy was sufficient to account for 0.72–1.03 m of surface ablation depending on the value of albedo assumed (Persson et al. 2001).

Figure 7e shows a 20-day averages of the ratio of ice speed to wind speed. Ratios were calculated from

3-h averages of ice speed with the inertial motion removed, and the wind speeds from anemometers on the 10-m meteorological towers. The drift ratios remained near the "free-drift" ratio of about 0.02, which indicates that internal ice stress gradients were less then those measured in previous experiments such as AIDJEX (McPhee 1980), which had winter drift ratios around .008%. The higher drift ratios for SHEBA suggest that internal ice stress gradients are not as important, and the SHEBA ice was relatively thinner, and consequently weaker. Also, it is likely that wind patterns were different between the two experiments (McPhee 2001).

Figure 8 shows examples of vertically resolved measurements that were collected over the entire annual cycle beginning with the rawinsonde temperatures in Fig. 8a, and the ice thickness and internal ice temperature measurements in Fig. 8b. The ice measurements were made at a site that was near the 20-m meteorological tower and was classified as undeformed, multiyear ice. The internal ice temperature is displayed using color contours; blues are colder and reds are warmer. The boundary between red and navy blue denotes the ice–ocean interface and the red–white boundary is the ice–air interface. The ice temperature contours show the propagation of the cold front through the ice in fall and winter and how the ice warmed starting in early March and eventually become isothermal in the summer. The gray shaded area on top represents the snow depth. Snow depth increased quickly in fall, then more slowly throughout winter, reaching a maximum of about 30 cm. Snowmelt was rapid and lasted only a few days in June. Ice thickness at this site increased from 1.8 m in October 1997 to 2.6 m in June 1998. During summer melt, there were 80 cm of surface ablation and 30 cm of bottom ablation at this location for a total loss of 110 cm in thickness. The melt season began shortly after atmospheric temperatures began to warm; the official first day of the melt season, 29 May, was marked by rainfall at the ice station. The atmospheric temperatures (Fig. 8a) below 3 km started warming at the beginning of May, about 30 days before the beginning of the melt.

Figures 8c and 8d show the temperature and salinity profiles through the top 80 m of the ocean. During the early part of the drift, across the abyssal plain of the Canada Basin, the mixed layer remained extremely fresh (minima of 26.41 psu), and the upward oceanic heat flux was small despite the presence of warm water just below the relatively shallow mixed layer. The extreme density gradient in the pycnocline effectively quelled turbulent entrainment even during the powerful storms in November and December.

The bathymetry in Fig. 8e suggest that the ice camp moved over several ocean regimes that affected both mixed layer and pycnocline properties. For example, warmer water within the pycnocline was encountered as the station drifted over the Northwind Ridge that contributed significantly to heat entrainment up through the mixed layer. These regional lateral gradients in upper-ocean properties explain the counterintuitive observation that the ocean mixed layer warmed somewhat during the winter between January and March. During the spring/summer melt season, the ice camp also drifted into regions where the advective increase in bulk mixed layer salinity dominated despite the injection of stabilizing meltwater into the upper mixed layer. The increases in salinity persisted until the top meter of freshwater from melting ice finally mixed downward around 6 August. There were additional effects from the variability of internal wave activity between Beaufort Sea and Northwind Ridge/Chukchi Cap regions that also contributed to modification of seasonal effects. These measurements preview the complexity that will be encountered in attempting to untangle the relative effects of atmospheric and ocean influences and seasonal versus regional effects on the energy budget of the ice pack in figure analyses.

Episodic and ancillary studies. There were a number of studies that were not carried out through the entire year, either because the measurements were season-specific processes, or because it was not logistically possible to make the measurements throughout the year. In addition, there were a number of studies that were not directly related to SHEBA objectives, (e.g., measurement of ozone), and a number of biological observations. Examples of some of these measurements are presented in this section.

Between May and October, more than a dozen helicopter survey flights were made around the ice station with a Nikon 35-mm camera, a video camera, and a KT-19 thermal radiometer that was mounted in a downward-looking orientation on the back of a helicopter's storage compartment (Perovich et al. 2001). Surveys were typically flown at an altitude of 1800 m under either clear skies or high clouds, so that the surface was not obscured. The flights covered a 50-km square box that was centered on the *Des Grossielliers.* Around two hundred 35-mm photographs (Fig. 9a) were taken on each flight, which were later assembled into mosaics documenting the temporal evolution of the ice cover on the aggregate scale. By digitizing the aerial photos and using image-processing software the photos were partitioned into

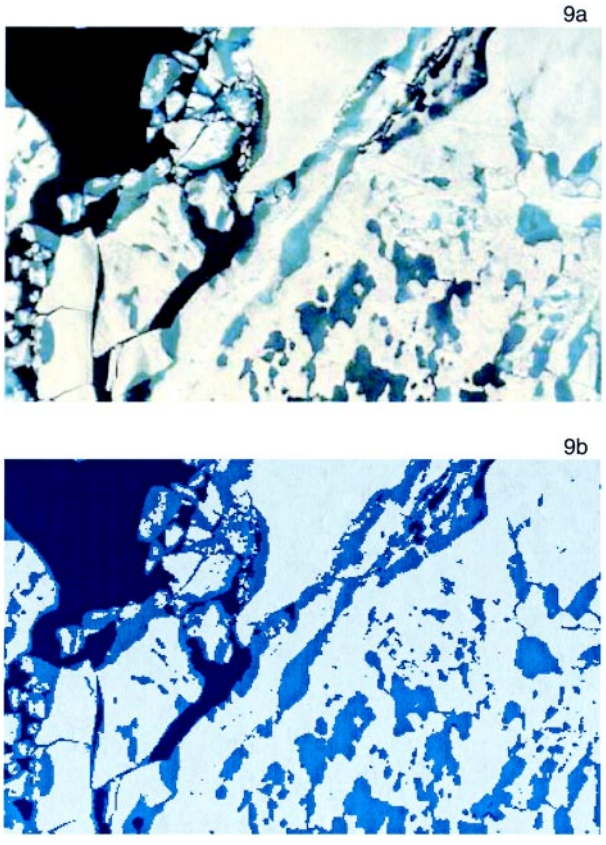

Fig. 9. (a) Aerial photography with 35-mm camera from helicopter; (b) classification of leads and open water (dark blue), meltponds (light blue), and ice (white) from digitized photo shown in (a).

areas of ice, ponds, and leads (Fig. 9b). After partitioning, the relative areas are computed, as well as perimeter and size distribution of ponds, leads, and floes. Combining these observations with results from process-oriented models makes it possible to generate area-averaged estimates of such quantities as albedo, solar heat input to the ice and ocean, ice concentration, pond fraction, and lateral melt rates.

Observations of total ozone content were made from the ship between 15 April and 31 May. The measurements were made every 2 h when the sun elevation was above 8° with a Russian standard filter ozonometer. This device measures and compares the direct and scattered radiation in a narrow spectral range between 300 and 320 nm, with an accuracy of 3%–8%, depending on the solar elevation angle. The magnitude of the total ozone measurements for the period was comparable with previous satellite and surface measurements from the Arctic Ocean region. Figure 10 shows the period between 20 April and 6 May when there was a short but dramatic decrease in ozone (460 to 360 Dobson units) that coincided with a period of strong solar activity, a phenomena that has been discussed by Shumilov et al.(1995).

Another unique measurement program at SHEBA was conducted with a tethered balloon. The balloon operated between December and July and was comprised of a 9 m^3 balloon that was attached to a 2-km-long Kevlar line that could be raised and lowered with the use of a winch. The "hot tether" allowed power to be sent up to the instrument packages and data to be transmitted down, including measurements of temperature, relative humidity, wind speed, and wind direction as well as cloud microphysical properties such as cloud droplet spectra and concentration from a cloud videometer. This instrument was valuable in documenting the detailed structure of strong inversions and large vertical gradients in the arctic boundary layer to much greater heights than the meteorological tower. Measurements of relative humidity and temperature around sunset on 23 March are shown in Fig. 11. The 8-month dataset collected by the balloon will allow detailed inspection of the seasonal changes in the boundary layer at the ice camp.

An important seasonal study was the measurement of the physical and optical properties made in a number of leads around the ice station during the summer months (Pegau and Paulson 1999). The measurements included surface maps (~0.15 m depth) of temperature and salinity using a CTD mounted on the bow of a small boat. Vertical profiles of temperature, salinity, absorption coefficient, and beam-attenuation coefficient of the water column were also collected. The measurements showed dramatic changes in temperature and salinity of the upper 2 m of water in the lead during the summer. At the beginning of the melt season, a layer of freshwater formed on the surface of the lead and this layer persisted and thickened for

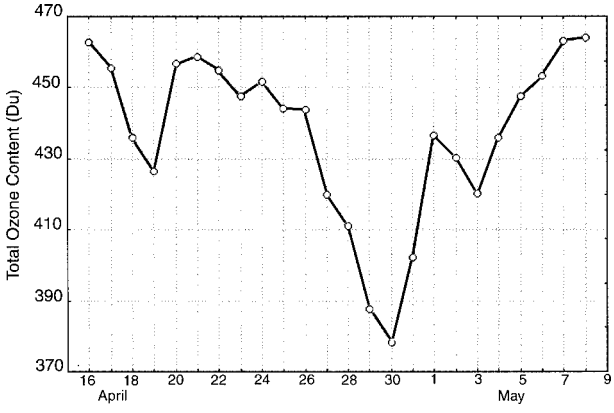

Fig. 10. Total ozone measured by a Russian standard filter ozonometer between 16 Apr and 8 May.

more than four weeks. Very low salinity and temperatures well above freezing characterized the freshwater layer (Fig. 12). The strong vertical stratification associated with the freshwater layer inhibited mixing until late July for the upper 15 m of the ocean, and until early August for the ocean mixed layer.

Biologists measured a wide variety of parameters, primarily from a winch stationed on the ice, with casts between the surface and the ocean floor (sometimes as deep as 4 km) throughout the year. Some of the primary variables were measurements of oxygen, phosphorus, nitrogen, silica, bacterial activity, and respiration rates of the total zooplankton community throughout the water column. Biological laboratories were distributed in three seatainers on the ice as well as on the ship; these facilitated year-round work experiments on plankton, radioisotopes, pollutants, and other variables. Changes in oxygen and nutrients, bacterial activity, and respiration rate of the total zooplankton community showed that the productivity of the Arctic Ocean at the SHEBA ice station was much higher than expected. It is possible that this may be the result of a thinning ice cover and more extensive leads, resulting in increased available solar radiation for production. An example of relative snow cover and surface chlorophyll (μg/liter in the 0–50 m layer) between 29 April and 24 June is shown in Fig. 13 and an (unrelated) inset shows an example of an 8-mm copepod, the dominant zooplankton species.

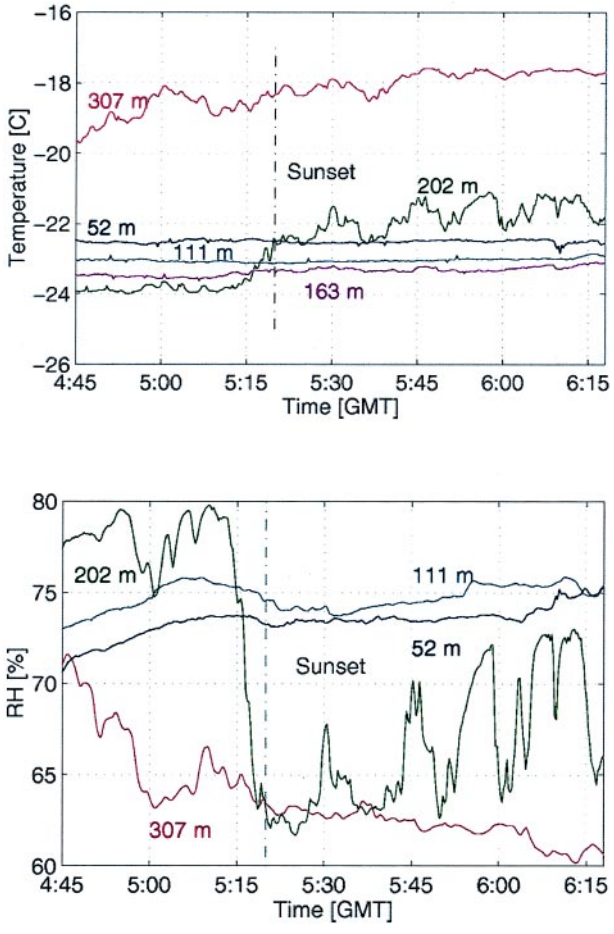

Fig. 11. Tethered balloon (top) temperatures at five levels, and (bottom) humidity at corresponding levels during sunset on 23 Mar 1998.

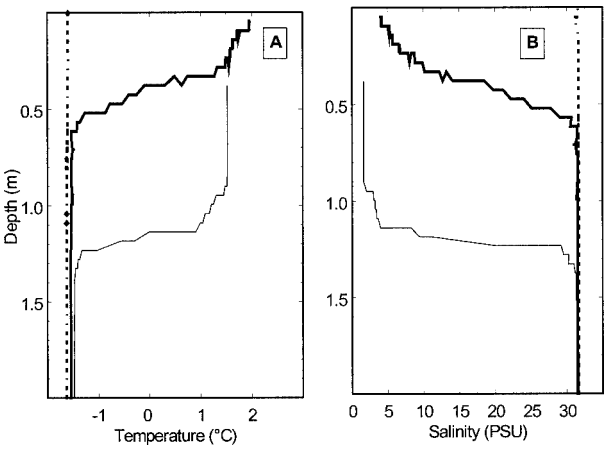

Fig. 12. Ocean CTD measurements in lead (a) temperature and (b) salinity. Profiles shown were collected on 19 Jun (dotted line), 11 Jul (thick line), and 22 Jul (thin line).

REPRESENTATIVENESS OF THE SHEBA YEAR. In light of the profound changes in the arctic environment that have occurred in the 1990s (Serreze et al. 2000), as well the fact that the SHEBA measurements will provide the baseline for a large number of process and model studies in coming years, it is important to assess how representative conditions were during SHEBA.

In the autumn of 1997 at the start of the SHEBA year, it was noted that the western Arctic appeared to be in an atypical state with an unusual lack of thick old ice. Recognizing that thin, first-year ice will melt earlier than old ice, McPhee et al. (1998) predicted a negative ice mass anomaly in the summer and autumn of 1998. This prediction proved to be accurate; 1998 was a record minimum in sea-ice extent in the western Arctic compared to historical records extending back to 1953 (Maslanik et al. 1999). During the summer of 1998, maximum seasonal distance between the ice edge and Point Barrow, Alaska (569 km), was 46% greater than the previous record year that occurred in the mid-1950s (390 km). Evidence indicates that negative sea-ice anomalies can be broadly understood in the context proposed by Rogers (1978) based on the composite analysis of summer-averaged sea level

pressure. Rogers found that light ice years tend to occur in conjunction with positive pressure anomalies over the northern Canadian Arctic Archipelago and north-central Siberia, and negative pressure anomalies over the east Siberian Sea. This pattern strengthens mean easterly and southerly winds over the Beaufort Sea and favors positive temperature anomalies, promoting melt and advection of ice to the west and north.

Other studies indicate that the patterns of pressure and ice drift have shifted counterclockwise 40°–60° from the historical patterns (Walsh et al. 1996; Morison et al. 1998; Steele and Boyd 1998) and that changes in the atmospheric have driven changes in the ocean, including shifts in the boundary between the eastern and western haloclines. During the SHEBA year, the position of the Beaufort high and the direction of the transpolar drift were similar to 1988–96 conditions, with the exception that the clear cyclonic circulation of ice out of the Kara and Laptev Seas region was absent. Another consequence of the combined oceanic and atmospheric influences during SHEBA was the low surface salinity in the Beaufort Sea, in addition to the minimum in ice thickness.

The initial observations made in the fall of 1997 indicated that the upper ocean was less saline and warmer than expected. The elevation of temperature above freezing of the ocean mixed layer during SHEBA had increased by a factor of 2.5 over that which occurred during AIDJEX. Additionally, the mixed layer salinity in 1997 was approximately 27.6 psu, compared to 29.7 psu in 1975 (Maykut and McPhee 1995; McPhee et al. 1998). From this data, and from a ^{7}Be tracer study (Kadko 2000) it was concluded that oceanic heat fluxes was considerably greater during the 1997 summer. Because the albedo of open water is considerably less than that of sea ice, it was suggested that the percentage of open water between 1975 and 1997 had tripled to allow a greater amount of heating to occur.

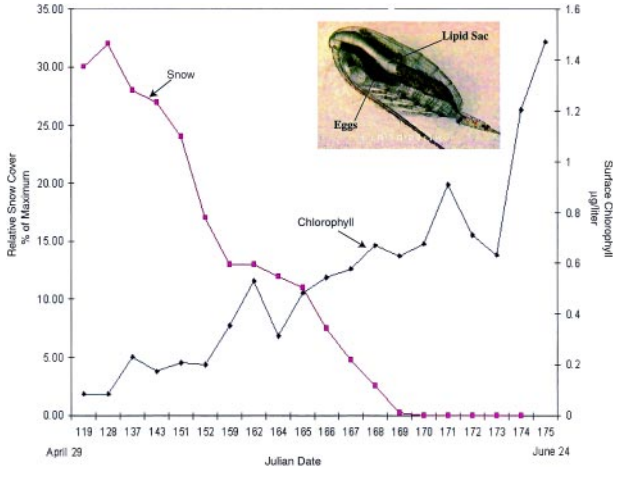

Fig. 13. Changes in ocean surface chlorophyll and snow cover over the biological growth season between 29 Apr and 24 Jun. Inset shows 8-mm copepod that was primary zooplankton species.

Air temperatures at SHEBA have been compared to a climatological surface temperature dataset that was produced by combining data from the drifting Russian NP stations and the U.S. arctic buoy program (Martin and Munoz 1997). Data were interpolated to the location of the SHEBA ice station and compared to SHEBA measured temperatures. This comparison indicated that the SHEBA year was slightly cooler than average in winter and warmer in spring. The SHEBA melt season lasted 78 days, compared to melt season durations calculated for the drifting Russian ice stations that ranged from 20 to 83 days and averaged 55 days (Lindsay 1998).

SHEBA PHASE III AND BEYOND. The goal of SHEBA Phase III (2000–20) is to utilize datasets collected during the field program to improve models of arctic ocean–atmosphere–ice processes, and to improve simulations of the present-day Arctic by utilizing coupled GCMs. The emphasis is on a multidisciplinary approach that addresses the integrated effects of ice, ocean, and atmospheric processes. The SHEBA Phase III project seeks to answer questions about the time- and space scales of air–sea–ice interactions and the individual and combined effects of various processes on present arctic climate. SHEBA Phase III is largely based upon the hypothesis that the principal uncertainties in arctic climate models are the ice–albedo feedback and cloud–radiation feedback; therefore, these are the primary processes under investigation. Toward this end, current research is focused on developing higher-order datasets, process studies, and development and testing of GCM parameterizations. To answer the questions that the SHEBA program has posed, results will be integrated over disciplinary boundaries, and collaborations between the observers and modelers will be essential. The SHEBA Phase III science projects are summarized in Table 4.

The SHEBA science team has implemented a data management strategy that has allowed timely access to the field data, with standardized documentation and formatting whenever possible, and extensive linkages with archives maintained by partner agencies have been negotiated. Over 100 SHEBA datasets can be accessed online at http://www.joss.ucar.edu/sheba/. These datasets, which are

Table 4. Phase III projects.

Description	Objective
Analyze atmospheric boundary layer data in regional model balance	Determine CRF mechanisms that affect the surface heat
Analyze atmospheric boundary layer and cloud data in an SCM	Develop parameterizations of CRF feedback mechanisms
Analyze aircraft data and test in an SCM, incorporate new parameterizations into a coupled SCM–GCM	Develop parameterizations of atmospheric, ice, radiation, and microphysical processes
Analyze observed atmospheric boundary layer data with nested mesoscale models	Determine the appropriate scale for GCM parameterizations
Analyze hydrographic data taken in leads and incorporate into a 2D convection model added to a ice–ocean submodel	Develop parameterizations of ocean mixed layer circulation in leads
Analyze hydrographic data taken in leads and incorporate into an LES turbulence model	Develop parameterizations of the heat flow in summer leads and the contribution to ice melt processes
Analyze ice data, and incorporate into process models to develop parameterizations, and then test in aggregate and GCM scale models	Develop parameterizations of IAF processes and incorporate into GCMs
Analyze ice and ocean data and incorporate into numerical models	Determine effects of ice–ocean exchanges in the IAF
Utilize ocean GCM coupled to sea-ice models to test parameterizations of upper ocean, and evaluate with observations	Develop parameterizations of upper-ocean processes and sea ice processes,
Single column modeling of the upper ocean and ice using observed datasets for forcing and evaluation	Develop a coupled sea-ice thickness–upper-ocean model, develop ice–ocean parameterizations, and examine effect of new parameterizations on the IAF
Analyze data with SCM and sea-ice models, and utilize the results in a GCM	Produce an improved simulation of arctic climate with a GCM
Aircraft data processing	Characterize cloud water contents
Surface boundary layer data processing	Characterize the atmospheric boundary layer properties
Merged satellite and aircraft data processing	Characterize surface properties and atmospheric conditions
Radar, lidar, and radiometer data processing	Characterize cloud microphysical, optical, and bulk properties

archived by the UCAR Joint Office for Scientific Support, will eventually be transferred to the National Snow and Ice Data Center that has primary responsibility for coordinating data holdings from field campaigns of the NSF Arctic Systems Science program. Information on the SHEBA program is maintained by the SHEBA project office online at http://sheba.apl.washington.edu/.

In addition to the specific objectives of SHEBA Phase III, it is likely that the detailed datasets from SHEBA Phase II will be important in directing further arctic research activities that will result from the heightened awareness of the role of the Arctic in global climate. Reconstructions from proxy data (e.g., tree rings and lake bed sediments) suggest a history of long-term climate change in the Arctic, but there

is evidence that over the past 400 years, the last 50 have been the warmest, suggesting an anthropogenic component. The last decade in particular appears to be a period where changes have accelerated, and have been observed throughout the ocean–ice–atmosphere–terrestrial–biological system. Areas of recent concern have included thinning of the Greenland ice sheet, retreat of arctic glaciers, thinning and decreased extent of the arctic sea ice, changes in the population distributions of marine mammals, changes in permafrost extent and snow extent, decreased CO_2 storage in soil, and a northward advance of tree line. These changes have been of sufficient magnitude to result in a letter signed in 1997 by 30 scientists from 17 U.S. institutions and 10 scientists from 8 institutions in six other countries, which has been endorsed by the Arctic System Science section of NSF. This letter has resulted in a series of workshops and is presently being carried forward in an interagency initiative named the Study of Environmental Arctic Change (SEARCH). It will be the objective of SEARCH to deploy a comprehensive campaign of long time series measurements in the Arctic, that will be combined with a program of process and model studies. A key element of SEARCH will be to continue and expand the interdisciplinary model utilized by SHEBA and to make coordinated measurements throughout the physical, biological, and social system to advance understanding of the arctic system. Information on the SEARCH program can be found online at http://psc.apl.washington.edu/search/.

ACKNOWLEDGMENTS. The NSF Arctic System Science (ARCSS) Program, under grants from the Office of Polar Programs, the Division of Ocean Sciences and the Division of Atmospheric Sciences, provides primary sponsorship for SHEBA. The Office of Naval Research (ONR) and the Japan Marine Science and Technology Center (JAMSTEC) also provided substantial direct support. SHEBA was conducted in partnership with the following organizations: DOE Atmospheric Radiation Measurement (ARM) program; NASA FIRE Arctic Cloud Experiment (FIRE-ACE) Project; RADARSAT Geophysical Processor System (RGPS) and the Alaska SAR Facility (ASF); Department of Fisheries and Oceans Canada; United States Coast Guard; and the Scientific Ice Expeditions (SCICEX) Project of the US Navy and NSF. SHEBA acknowledges the invaluable contributions of the crew and captains of the Canadian Coast Guard ship *Des Grossielliers* in providing a secure, superbly equipped, comfortable, and congenial base of operations for the SHEBA program. Essential transportation, setup, and breakdown support were provided by the crew and captains of the Canadian Coast Guard ship *Louis St. Laurent,* and the U.S. Coast Guard ships *Polar Star* and *Polar Sea.* A program the size and scope of SHEBA would not be possible without the dedicated efforts of a large number of scientists, engineers, technicians, programmers, support staff, and logistic crews that are too numerous to be named; to all of these individuals the authors extend deep appreciation. The scope of the SHEBA project is considerably extended by partner programs both in the United States and in Japan, Canada, and Russia.

REFERENCES

Andreas, E. L, P. S. Guest, P. O. G. Persson, C. W. Fairall, T. W. Horst, and R. E. Moritz, 2002: Near-surface water vapor over polar sea ice is always near ice-saturation. *J. Geophys. Res.,* in press.

Curry, J. A., 1983: On the formation of continental polar air. *J. Atmos. Sci.,* **40,** 2279–2292.

——, W. B. Rossow, D. Randall, and J. L. Schramm, 1996: Overview of arctic cloud and radiation characteristics. *J. Climate,* **9,** 1731–1764.

——, and Coauthors, 2000: FIRE Arctic Clouds Experiment. *Bull. Amer. Meteor. Soc.,* **81,** 5–29.

Han, W., K. Stamnes, and D. Lubin, 1999: Remote sensing of surface and cloud properties in the Arctic from AVHRR measurements. *J. Appl. Meteor.,* **38,** 989–1012.

Intrieri, J. M., M. D. Shupe, T. Uttal, and B. J. McCarty, 2002: An annual cycle of arctic cloud characteristics observed by radar and lidar at SHEBA. *J. Geophys. Res.,* in press.

Kadko, D., 2000: Modeling the evolution of the arctic mixed layer during the fall 1997 SHEBA project using measurements of 7Be. *J. Geophys. Res.,* **105,** 3369–3378.

Kahl, J. D., 1990: Characteristics of the low-level temperature inversion along the Alaskan Arctic coast: 1990. *Int. J. Climatol.,* **10,** 537–548.

——, N. A. Zaitseva, V. Khattatov, R. C. Schnell, D. M. Bacon, J. Bacon, V. Radionov, and M. C. Serreze, 1999: Radiosonde observations from the former Soviet "North Pole" series of drifting ice stations, 1954–90. *Bull. Amer. Meteor. Soc.,* **80,** 2019–2026.

Lindsay, R. W., 1998: Temporal variability of the energy balance of thick arctic pack ice. *J. Climate,* **11,** 313–331.

Manley, T. O., and K. Hunkins, 1985: Mesoscale eddies of the Arctic Ocean. *J. Geophys. Res.,* **90,** 4911–4930.

Martin, S., and E. A. Munoz, 1997: Properties of the arctic 2-meter air temperature field for 1979 to the present derived from a new gridded dataset. *J. Climate,* **10,** 1428–1440.

Maslanik, J. A., M. C. Serreze, and T. Agnew, 1999: On the record reduction in 1998 western arctic sea ice cover. *Geophys. Res. Lett.,* **26,** 1905–1908.

——, J. Key, C. W. Fowler, T. Nguyen, and X. Wang, 2001: Spatial and temporal variability of satellite-derived cloud and surface characteristics during FIRE ACE. *J. Geophys. Res.,* **106** (D14), 15 233–15 249.

Maykut, G. A., and M. G. McPhee, 1995: Solar heating of the arctic mixed layer. *J. Geophys. Res.,* **100,** 24 691–24 703.

McPhee, M. G., 1980: An analysis of pack ice drift in summer. *Sea Ice Processes and Models,* R. Pritchard, Ed., University of Washington Press, 62–75.

——, 2002: Turbulent stress at the ice/ocean interface and bottom surface hydraulic roughness during the SHEBA drift. *J. Geophys. Res.,* in press.

——, T. P. Stanton, J. H. Morison, and D. G. Martinson, 1998: Freshening of the upper ocean in the central Arctic: Is perennial ice disappearing? *Geophys. Res. Lett.,* **25,** 1729–1732.

Morison, J. H., M. Steele, and R. Andersen, 1998: Hydrography of the upper Arctic Ocean measured from nuclear submarine USS Pargo. *Deep-Sea Res.,* **45,** 15–38.

Moritz, R. E., J. A. Curry, N. Untersteiner, and A. S. Thorndike, 1993: Prospectus: Surface heat budget of the Arctic Ocean. NSF-ARCSS OAII Tech. Rep. 3, 33 pp. [Available from the SHEBA Project Office, Polar Science Center, Applied Physics Laboratory, University of Washington, Seattle, WA 98105.]

Pegau, W. S., and C. A. Paulson, 1999: The role of summer leads in the heat and mass balance of the upper Arctic Ocean. Preprints, *Fifth Conf. on Polar Meteorology and Oceanography,* Dallas, TX, Amer. Meteor. Soc., 401–403.

Peixoto, J. P., and A. H. Oort, 1992: *Physics of Climate.* American Institute of Physics, 520 pp.

Perovich, D. K., and Coauthors, 1999: The surface heat budget of the Arctic Ocean. *Eos, Trans. Amer. Geophys. Union,* **80,** 481–486.

——, W. B. Tucker III, and K. A. Ligett, 2002: Aerial observations of the evolution of ice surface conditions during the summer. *J. Geophys. Res.,* in press.

Persson, P. O. G., C. W. Fairall, E. L Andreas, and P. S. Guest, 2002: Measurements near the atmospheric surface flux group tower at SHEBA; Near-surface conditions and surface energy budget. *J. Geophys. Res.,* in press.

Randall, D., and Coauthors, 1998: Status of and outlook for large-scale modeling of atmosphere–ice–ocean interactions in the Arctic. *Bull. Amer. Meteor. Soc.,* **79,** 197–219.

Rogers, J. C., 1978: Meteorological factors affecting interannual variability of summertime ice extent in the Beaufort Sea. *Mon. Wea. Rev.,* **106,** 890–897.

Rossow, W. B., A. W. Walker, and L. C. Garder, 1993: Comparison of ISCCP and other cloud amounts. *J. Climate,* **6,** 2394–2418.

Schweiger, A. J., and J. R. Key, 1994: Arctic Ocean radiative fluxes and cloud forcing as estimated from the ISCCP C2 dataset, 1983–1990. *J. Climate Appl. Meteor.,* **33,** 948–963.

Serreze, M. C., J. D. Kahl, and R. C. Schnell, 1992: Low-level temperature inversions of the Eurasian Arctic and comparisons with Soviet drifting station data. *J. Climate,* **5,** 615–629.

——, and Coauthors, 2000: Observational evidence of recent changein the northern high-latitude environment. *Climatic Change,* **46,** 159–207.

Shumilov, I., E. A. Kasatkina, K. Henriksen, and O. M. Raspopov, 1995: Ozone "miniholes" initiated by energetic solar photons. *J. Atmos. Terr. Phys.,* **6,** 665–671.

Shupe, M. D., T. Uttal, S. Y. Matrosov, and A. S. Frisch, 2001: Cloud water contents and hydrometer sizes during the FIRE-Arctic Clouds Experiment. *J. Geophys. Res.,* **106,** 15 015–15 028.

Stamnes, K., R. G. Ellingson, J. A. Curry, J. E. Walsh, B. D. Zak, 1999: Review of science issues, deployment strategy, and status for the ARM North Slope of Alaska—Adjacent Arctic Ocean climate research site. *J. Climate,* **12,** 46–63.

Steele, M., and T. Boyd, 1998: Retreat of the cold halocline layer in the Arctic Ocean. *J. Geophys. Res.,* **103,** 10 419–10 435.

Stern, H. L., and R. E. Moritz, 2002: Sea ice kinematics and surface properties from RADARSAT SAR during the SHEBA drift. *J. Geophys. Res.,* in press.

Stokes, G. M., and S. E. Schwartz, 1994: The Atmospheric Radiation Measurement (ARM) program: Programmatic background and design of the Cloud and Radiation Testbed. *Bull. Amer. Meteor. Soc.,* **75,** 1201–1221.

Vowinkel, E., and S. Orvig, 1970: The climate of the north polar basin. *Climates of the Polar Regions,* S. Orvig, Ed., World Survey of Climatology Series, Vol. 14, Elsevier, 129–152.

Walsh, J. E., W. L. Chapman, and T. L. Shy, 1996: Recent decrease of sea level pressure in the central Arctic. *J. Climate,* **9,** 480–486.

Warren, S. G., C. J. Hahn, J. London, R. M. Chervin, and R. L. Jenne, 1988: Global distribution of total cloud cover and cloud type amounts over the ocean. NCAR Tech. Note NCAR/TN-317+STR, 212 pp.

EYEWITNESS

Evolution of the Atmospheric Sciences

by ROBERT G. FLEAGLE

Eyewitness: Evolution of the Atmospheric Sciences describes how the atmospheric sciences were transformed in the span of the author's professional career from its origins in primitive weather forecasting to its current focus on numerical modeling of environmental change. It describes the author's observations of persons, events, and institutions beginning with graduate study during the Second World War and moving on to continuing expansion of the atmospheric sciences and technologies, through development of a major university department, development of new scientific and professional institutions, and to the role that the science of the atmosphere now plays in climate change and other issues of social and political policy.

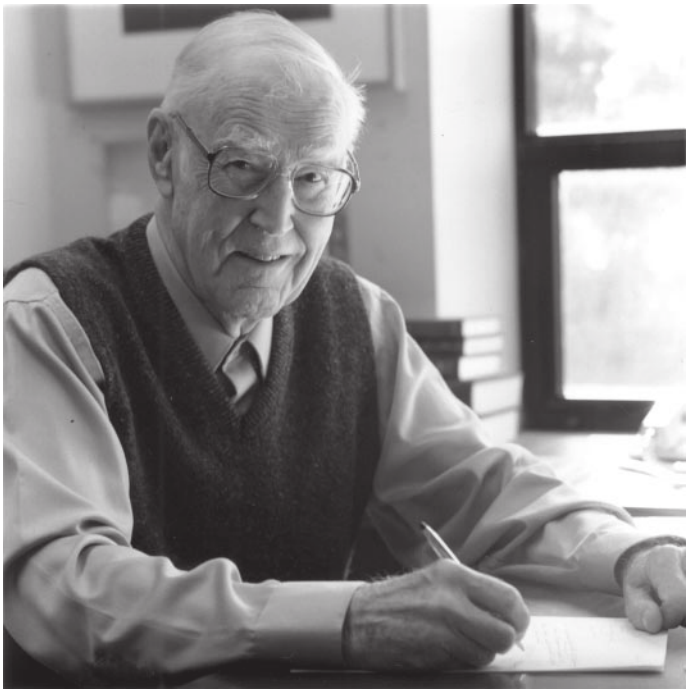

Photo ©Kathy Sauber/University of Washington

EYEWITNESS: EVOLUTION OF THE ATMOSPHERIC SCIENCES
ISBN 1-878220-39-X, 129 pp., hardbound, $65 list/$45 member. To place an order, submit your prepaid orders to: Order Department, AMS, 45 Beacon Street, Boston, MA 02108-3693; call 617-227-2425 to order by phone using Visa, Mastercard, or American Express; or send e-mail to amsorder@ametsoc.org. Please make checks payable to the American Meteorological Society.

ABOUT THE AUTHOR

Robert G. Fleagle earned degrees in physics and meteorology at The Johns Hopkins University and New York University and began his professional career in 1948 at the University of Washington (UW). His research has focused on the structure of midlatitude cyclones, the physics and structure of the surface boundary layer, and processes of air–sea interaction. He is the author of about 100 papers published in scientific journals and of books on atmospheric physics and global environmental change. Applications of science to social and political policy have been important motivations for his career and have occupied his attention increasingly as the decades passed.

Fleagle participated at close range in the beginnings and growth of a major university department and of the University Corporation for Atmospheric Research (UCAR). In 1963 and 1964 he served as a staff specialist in the Office of Science and Technology, Executive Office of the President, and in 1977–78 he served as consultant to the National Oceanic and Atmospheric Administration. He has held many administrative posts including chairman of the UW Department of Atmospheric Sciences (1967–77), chairman of the National Academy of Sciences Committee on Atmospheric Sciences (1969–73),